Turkish Computational and Theoretical Chemistry

Turkish Comp Theo Chem (TC&TC)

Volume(Issue): 10(1) – Year: 2026 – Pages: 101-109

e-ISSN: 2602-3237

https://doi.org/10.33435/tcandtc.1615590

Received: 08.01.2025 **Accepted:** 26.03.2025 *Research Article*

The Therapeutic Potential of Methanolic Leaf Extract of Syzygium cumini in Managing Type 2 Diabetes Mellitus based on Network Pharmacology Study

Muhammad Arba[a,1], Sunandar Ihsan[a], Rurianti Ramlah Udin[b], Ahmad Najib[b], Firzan Nainu[c], Muhammad Sulaiman Zubair[d]

[a]Department of Pharmaceutical Analysis and Medicinal Chemistry, Faculty of Pharmacy, Universitas Halu Oleo, Kendari, Indonesia

[b]Department of Natural Product Chemistry, Faculty of Pharmacy, Universitas Muslim Indonesia.

[c]Department of Pharmacy, Faculty of Pharmacy, Hasanuddin University, Makassar, Indonesia 90245

[d]Department of Pharmacy, Faculty of Sciences, Tadulako University, Palu, Indonesia

Abstract: Type 2 diabetes mellitus (T2DM) is a significant metabolic disorder affecting approximately 537 million people globally. Syzygium cumini is a herbal plant with multitarget and multi-pathway potential, used traditionally in medicine due to its diverse pharmacological properties. Therefore, this study aimed to predict the target profiles and pharmacological mechanisms of S. cumini compounds using network pharmacology. The methanolic leaves extract of S. cumini was analyzed using LC-HRMS, ADMET prediction, network pharmacology, and molecular docking. LC-HRMS analysis identified 42 compounds in the extract and 35 satisfied Lipinski's rule of 5. From the analysis, 150 common targets for S. cumini were identified, leading to the determination of 10 core targets, namely IL-6, TNF, ALB, AKT1, IL1B, STAT3, CTNNB1, PPARG, TLR4, and PTGS2. Molecular docking was then carried out on the compounds focusing on the three best targets, namely IL-6, TNF, and ALB. A total of 4, 4, and 1 compounds targeted IL-6, TNF-α, and ALB, respectively. In particular, bergenin and FF-MAS had binding energy comparable to native ligand when bound to IL-6 and TNF-α, respectively. NP-012381 was the only compound had lower binding energies than native ligand on the three targets (IL-6, TNF-α, and ALB) simultaneously. This present study showed the potential of S. cumini in inhibiting T2DM.

Keywords: Syzygium cumini, computational study, interleukin, tumor necrosis factor, albumin

Graphical abstract:

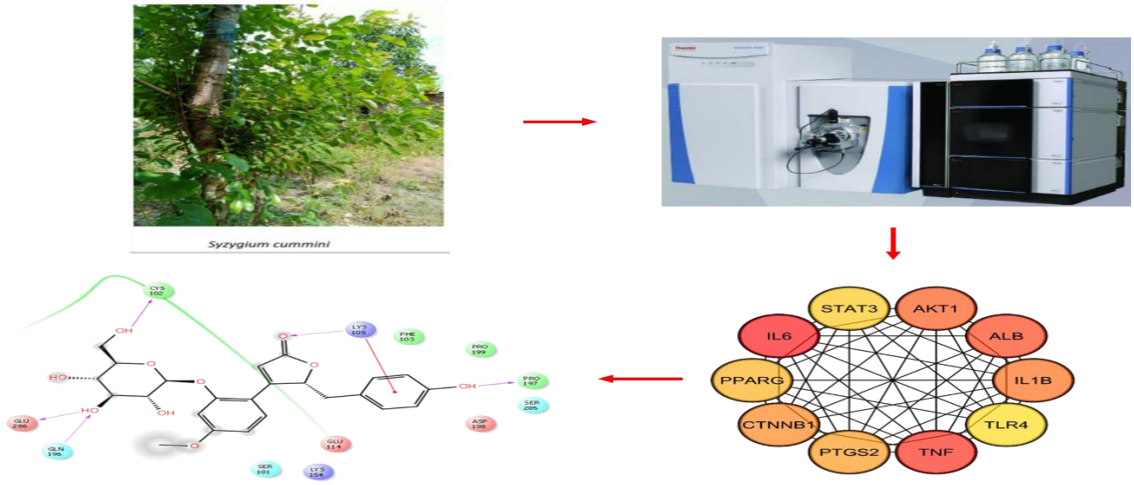

[1] Corresponding Authors

e-mail: muh.arba@uho.ac.id

1. Introduction

Diabetes mellitus (DM), characterized by elevated blood sugar levels, is a significant global public health issue, affecting approximately 537 million people worldwide [1]. The most prevalent form of this disease is type 2 diabetes mellitus (T2DM), accounting for over 90% of all cases. T2DM is marked by insulin resistance and dysfunction of pancreatic β-cells [2], which contributes to glycotoxicity and various systemic complications [3]. Current clinical treatments for T2DM, such as metformin and thiazolidinediones [4] are associated with serious side effects, including hypoglycemia and gastrointestinal disturbances [5]. However, herbal plants are known for minimal side effects and high safety profile, showing the potential as sources for developing new T2DM therapies [6].

Several studies have shown the biological activities of *Syzygium cumini*. The various parts of *S. cumini* exhibit significant biological activity and hold the potential for developing products applicable to the pharmaceutical and food industries. In 2020, Kandeda et al. (2022) suggested that the aqueous extract of *S. cumini* had antiepileptic- and anti-amnesic-like effects, which were mediated in part by antioxidant and anti-inflammatory activities [7]. Abdin et al. (2020) implied the antioxidant and anti-inflammatory activities of target anthocyanins di-glucosides isolated from *S. cumini* [8]. Sing et al (2018) reported that *S. cumini* was rich in phenolic acids, (gallic and ellagic acid), flavonoids (quercetin, myricetin, flavonol glycosides, anthocyanins, flavonols, flavanols, and flavanonols), tannins (mostly ellagitannins), and anthocyanins (delphinidin, petunidin, and malvidin in glycosylated forms). Due to this components, the plant functions as anti-inflammatory, anti-allergic, antihyperglycaemic, anticancer, cardioprotective, radioprotective, antibacterial, chemopreventive, and antioxidant agent [9]. Srivastava and Chandra (2013) also reported that *S. cumini* had beneficial physiological effects, including antidiabetic properties [10]. Despite these results, no network pharmacology studies have investigated the pharmacological effects of the chemical compounds on multiple targets and pathways as anti-T2DM agent. Network pharmacology underscores a paradigm shift from the "one compound, one target" paradigm to a novel version of the "multi-components, multi-target," strategy [11]. This network pharmacology is particularly suitable for addressing the mechanism of action of a herbal plant considering its multiple chemical compounds [11]. Therefore, this study applied a network pharmacology method to enhance the molecular understanding of *S. cumini* potential as anti-T2DM agent in a multidrug and multitarget paradigm [12]

2. Computational Method

2.1. Plant Material and Extraction Process, LC-HRMS Analysis, and ADME Prediction

S. cumini leaves were collected in June 2024 from Kalebarembeng Village, Bontonompo Subdistrict, Gowa Regency, South Sulawesi Province, Indonesia (coordinates: 5°18'21"S, 119°23'48"E). Leaves were cleaned using wet sorting to remove impurities, washed, thinly sliced, and air-dried. The crude *S. cumini* simplicia extract (300 g) was subjected to two rounds of maceration using ethanol as the solvent, yielding a crude extract of 5.62 g, with a percentage of 1.87% (w/w).

High-resolution mass spectrometry analysis was carried out using liquid chromatography (LC-HRMS) following the method described by Zubair et al. (2021) [13]. ADMET properties of the compounds were predicted using SwissADME web server (http://www.swissadme.ch/) as outlined by Daina et al. (2017) [14].

2.2. Genes Identification Associated with Type 2 Diabetes Mellitus

Target prediction for the compounds of *S. cumini* was conducted using SwissTargetPrediction and SEA databases (https://sea.bkslab.org) (https://sea.bkslab.org) by inputting SMILES code for each compound [15, 16]. Genes associated with T2DM were predicted using OMIM database (https://www.omim.org), DisGeNET, and GeneCards (https://www.genecards.org) [17-19]. The GeneCards data were filtered to include the top 500 targets [20]. Subsequently, the results of the disease targets and compounds were filtered and combined into a Venn diagram using Bioinformatics and System Biology (https://bioinformatics.psb.ugent.be/webtools/Venn).

2.3. Protein-Protein Interaction (PPI) Network and Core Target Selection

Protein-protein interaction (PPI) network was constructed using STRING database (https://string-db.org), with the target proteins restricted to the species *Homo sapiens* and a high confidence threshold of 0.007. In this case, other parameters were left at the default settings. The resulting PPI network was imported into Cytoscape v3.10.2 Cytoscape v3.10.2 [21] for further analysis.

2.4. GO Analysis and KEGG Path

Gene Ontology (GO) analysis was conducted using Metascape (https://www.metascape.org) and shinyGO 0.80 databases to evaluate the biological functions, cellular processes, and molecular components associated with the predicted protein targets [22-24]. Additionally, KEGG (Kyoto Encyclopedia of Genes and Genomes) pathway analysis was carried out to identify the metabolic pathways or molecular signaling processes influenced by the compounds and the targets in *S. cumini* and T2DM. The resulting pathways were used as a working framework to study the effects of the compounds.

2.5. Molecular Docking

The crystal structures of IL-6, TNF-α, and ALB were used as protein targets for docking simulations. The 2D structures of the *S. cumini* compounds identified through LC-HRMS analysis were converted into 3D using Maestro LigPrep module with OPLS_2005 force field [25]. Protein and ligand preparations were carried out based on previously established protocols [26, 27] using Maestro Schrödinger 11.1.012 release 2017-1 software (Schrödinger, New York, NY, USA) [25]. Prednisolone was used as a positive control for docking to IL-6, following the procedure described in the previous study [28].

3. Results and discussion

3.1. LC-HRMS Analysis

LC-HRMS analysis of *S. cumini* extracts identified 42 compounds. All compounds were screened for ADME properties, with 35 meeting the Lipinski rule criteria, as shown in Tables S1 and S2.

3.2. The Target Genes of *S. cumini* Compounds and T2DM

The target proteins from SwissTargetPrediction and SEA databases identified for *S. cumini* were 990 and 439, respectively, while gene targets for T2DM from the GeneCards, DisGeNet, and OMIM databases were 500, 271, and 82, respectively. After eliminating duplicates, 1,138 unique targets of the *S. cumini* compounds were obtained. Similarly, 850 gene targets associated with T2DM have been identified using OMIM, DisGeNET, and GeneCards databases. By comparison, using a Venn diagram, 150 common targets shared between *S. cumini* and T2DM were identified, as shown in Figure 1.

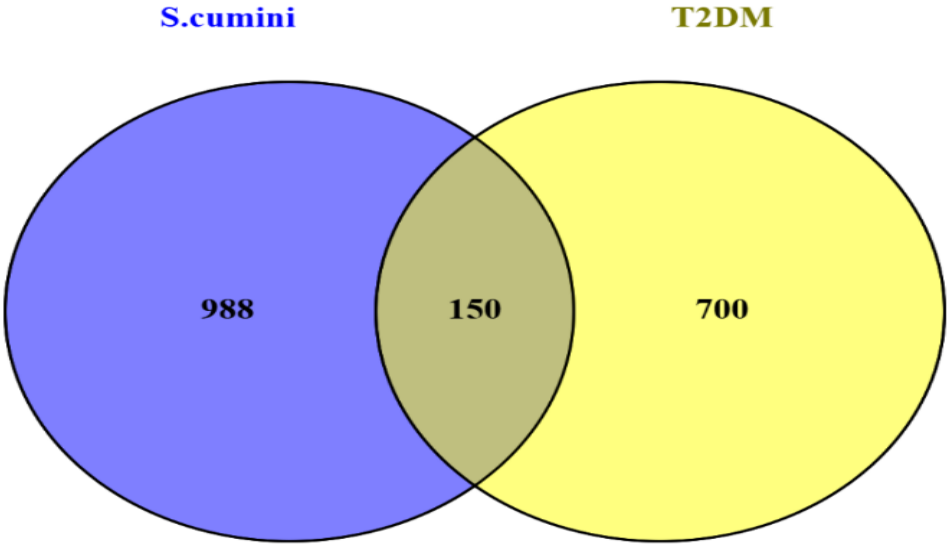

Figure 1. Venn diagram of a common target of T2DM- *S. cumini*. The blue, yellow, and dark colors represent genes of T2DM, compounds of *S. cumini*, and the common target, respectively

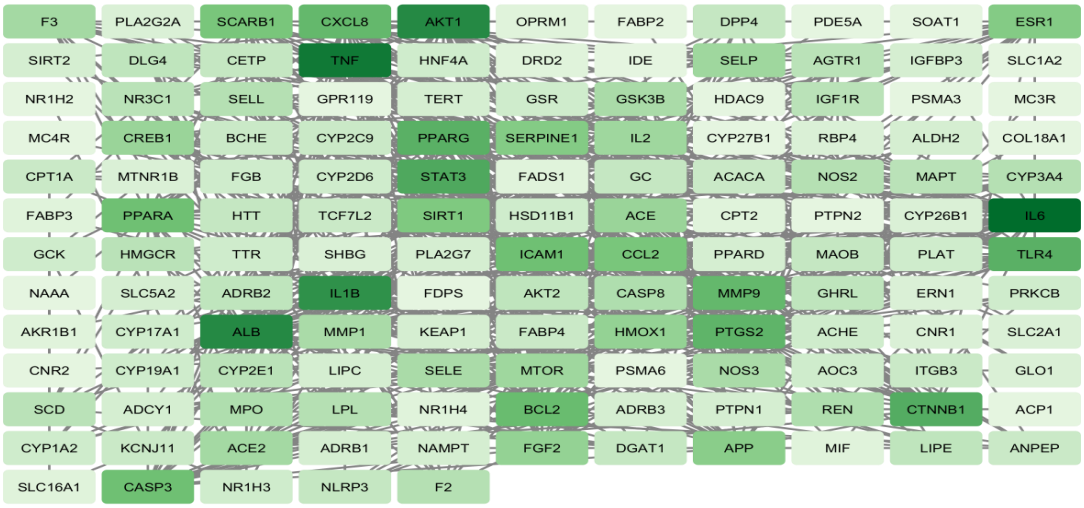

Figure 2. Visualization of PPI network for *S. cumini* and T2DM, where the intensity of the green color shows the significance of gene degree

Table 1. The values of degree, closeness centrality, and betweenness centrality of the top 10 proteins.

NO	Name	Degree	Closeness Centrality	Betweenneess Centrality
1	IL-6	44	0.536	0.08724512636608397
2	TNF	41	0.5381526104417671	0.09789594317925121
3	ALB	37	0.536	0.15564233230351093
4	AKT1	37	0.5173745173745175	0.13313266304234703
5	IL1B	35	0.5153846153846153	0.03840495031775519
6	STAT3	29	0.47017543859649125	0.03069596291814518
7	CTNNB1	28	0.48201438848920863	0.0642811157937861
8	PPARG	27	0.48201438848920863	0.09701829683867383
9	TLR4	27	0.47686832740213525	0.013584118528804279
10	PTGS2	26	0.48727272727272725	0.04911658338795967

3.3. Protein-Protein Interaction (PPI)

PPI network was constructed using the Search Tool for the Retrieval of Interacting Genes/Proteins (STRING) (http://string-db.org). The resulting network was analyzed using Cytoscape v3.10.2 (https://cytoscape.org). Key proteins with the highest number of interactions were identified, including IL-6, TNF, ALB, AKT1, IL1B, STAT3, CTNNB1, PPARG, TLR4, and PTGS2, as shown in Figure 2.

The core targets were identified based on Degree, Closeness, and betweenness values using the CytoHubba plug-in (Table 1), resulting in a network comprising 129 nodes and 599 edges. The analysis consistently showed IL-6, TNF, ALB, AKT1, IL1B, STAT3, CTNNB1, PPARG, TLR4, and PTGS2 as key targets (Figure S1). Table 1 shows the top 10 proteins along with the Degree, Closeness Centrality, and Betweenness Centrality values.

Higher degree values show a greater number of direct connections, reflecting a more significant role of the protein. Similarly, higher betweenness centrality values suggested that the protein serves as a critical node for facilitating communication. Higher closeness centrality values represent an advanced level of centrality and faster signal transmission to other nodes in the network [29].

3.4. KEGG and GO Analysis

Functional analysis was carried out using KEGG and GO across three categories, namely biological process (BP), cellular component (CC), and molecular function (MF). Figures 4 and S2 show the top 20 enriched terms for each category ranked by p-value. The highest-ranking terms are the

regulation of hormone levels, phagocytic cup, and aromatase binding for GO biological process, cellular component, and molecular function.

AGE-RAGE signaling pathway in diabetic complications was reflected in KEGG pathway as shown in Figure 5.

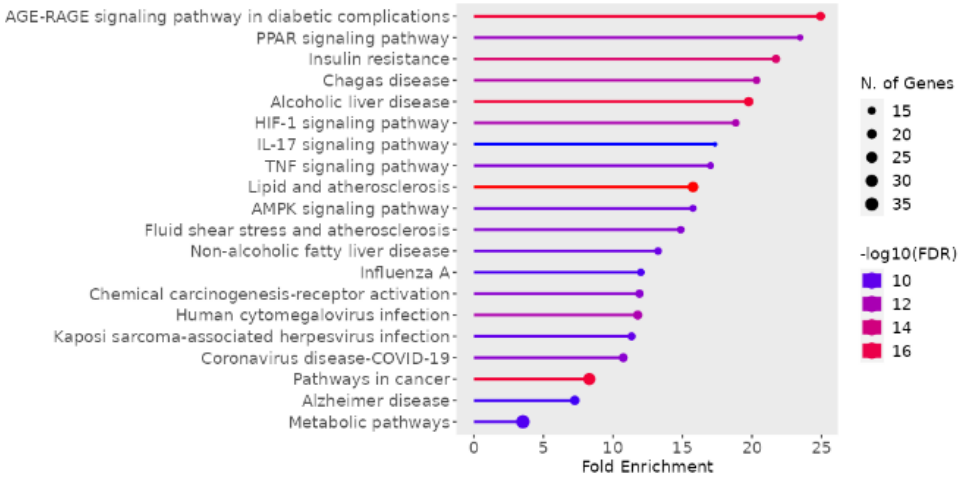

Figure 4. The top 20 enriched terms for KEGG pathway ranked by p-value.

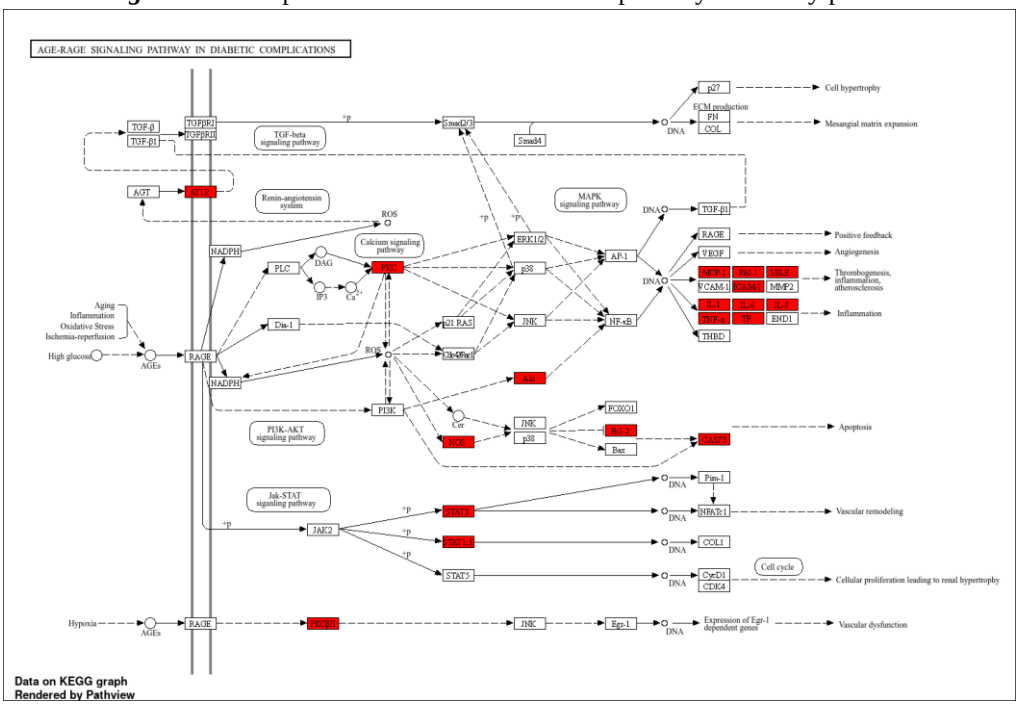

Figure 5. KEGG pathway of T2DM, in which the red color represents genes in the common target

The advanced glycation end (AGE) products are formed when the free amino groups of proteins react with carbonyl groups of sugars [30]. AGE and receptor (RAGE) signalling pathway was shown to play a role in diabetes [31, 32]. According to a previous study, the level of AGE was increased in diabetes [33]. In a hyperglycemic environment, tissue glucose levels rise, causing the peripheral nervous system to produce AGE. Diabetes greatly facilitates the production and accumulation of AGE because glucose serves as the primary source of carbonyl groups for glycation processes. AGE receptors may also play a part in the development of diabetes complications, in addition to the buildup of AGE in tissues. AGE has been shown to bind to several receptors, such as RAGE.

3.5. Molecular Docking

The network pharmacology results identified 10 core targets, and the three best were selected for

molecular docking, namely IL-6, TNF-α, and ALB. There were 4 compounds targeting IL-6, namely 18-β-Glycyrrhetinic, ursolic, bergenin, and NP-012381. A total of 4 compounds were targeting TNF-α, namely 4-(4-methylpiperidin-1-yl)benzoic acid, 18-β-Glycyrrhetinic acid, FF-MAS, Comp29, and NP-012381, while only 1 (NP-012381) targeted ALB. Molecular docking was then carried out on the compound to indentify the binding affinity to its corresponding target [34-37], as shown in Table 3.

Table 3. Binding energies for each compound to its corresponding target

Compound	**Binding energy (kcal/mol)**		
	IL-6 (PDB ID : 1N26)	**TNF (PDB ID : 2AZ5)**	**ALB (PDB ID : 1E7A)**
Native ligand (Prednisolone)	-4.180		
18-β-Glycyrrhetinic acid	-2.489		
Ursolic acid	-1.808		
Bergenin	-4.513		
NP-012381	-5.923	-5.186	-6.116
Native ligand (307)		-3.348	
4-(4-methylpiperidin-1-yl)benzoic acid		-2.381	
FF-MAS		-3.217	
Comp 29		-2.084	
Native ligand (PFL)			-6.078

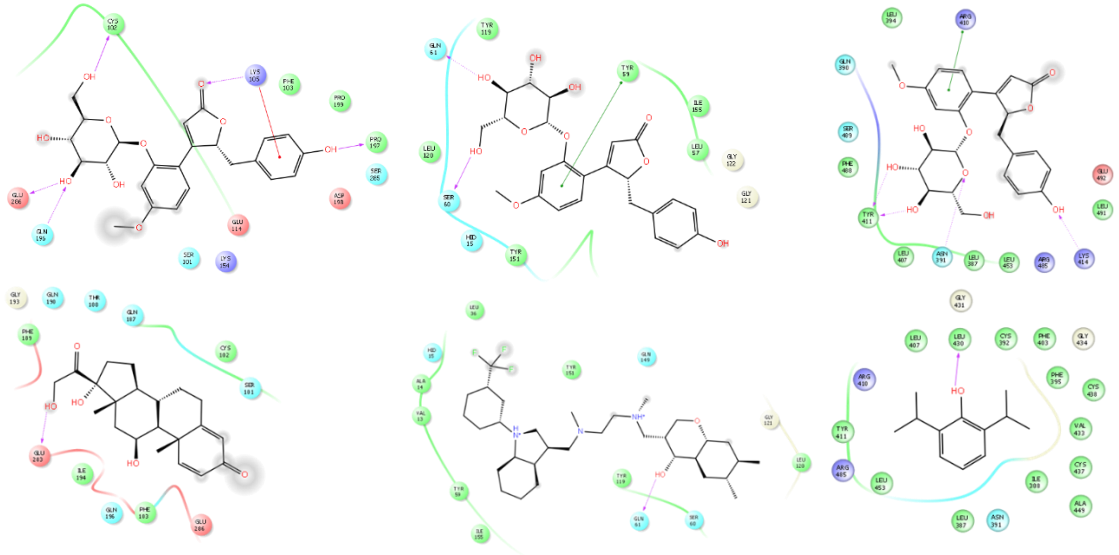

The docked poses to IL-6: NP-012381 (top) and prednisolone (bottom)

The docked poses to TNF-α: NP-012381 (top) and 307 (bottom)

The docked poses to ALB: NP-012381 (top) and PFL (bottom)

Figure 5: The docked poses of NP-012381 and native ligand to IL-6, TNF-α, and ALB

Binding energy of native ligand (prednisolone) to interleukin-6 (IL-6) was -4.180 kcal/mol, while those of 18-β-Glycyrrhetinic, Ursolic, Bergenin, and NP-012381 were -2.489 kcal/mol, -1.808 kcal/mol, -4.513 kcal/mol, and -5.923 kcal/mol, respectively. Similarly, binding energies of ligand to TNF-α were -2.381 kcal/mol, -1.734 kcal/mol, -3.217 kcal/mol, -2.084 kcal/mol, and -5.186 kcal/mol for 4-(4-methylpiperidin-1-yl)benzoic acid, 18-β-Glycyrrhetinic acid, FF-MAS, Comp 29, and NP-012381, respectively, In the case of native ligand (307) of TNF-α, binding energy was -3.348 kcal/mol. Binding energy of native ligand (PFL) and NP-012381 to ALB were -6.078 and -6.116 kcal/mol, respectively.

Bergenin and FF-MAS had binding energies comparable to those of native ligand when bound to IL-6 and TNF-α, respectively. NP-012381 was the only compound targeting IL-6, TNF-α, and ALB simultaneously, and binding energy was lower than native ligand. Figure 5 shows the docked poses of NP-012381 and native ligand to IL-6, TNF-α, and ALB. In addition, Figure S3 shows the docked pose of each compound to its corresponding target.

4. Conclusions

In conclusion, the present study investigated the potential of S. cumini methanolic leaf extract as a therapeutic agent for type 2 diabetes mellitus (T2DM). The findings demonstrated that the extract contains bioactive compounds with significant potential to inhibit key proteins associated with T2DM, including IL-6, TNF-α, ALB, AKT1, IL1B, STAT3, CTNNB1, PPARG, TLR4, and PTGS2. These proteins play critical roles in the pathophysiology of T2DM by contributing to AGE-RAGE signaling pathway in diabetic complications. Molecular docking analysis carried out on the three best targets showed that bergenin and FF-MAS had comparable binding energy with native ligand when bound to IL-6 and TNF-α, respectively. However, NP-012381 was a potential inhibitor of IL-6, TNF-α, and ALB simultaneously, as evidenced by its lower binding energy than native ligand. Overall, this study emphasizes the potential of S. cumini methanolic leaf extract as a promising candidate for the development of novel, multi-target treatments for T2DM.

Acknowledgments

The author (MA) is grateful to Hibah Kolaborasi Penelitian Strategis (Katalis) Kemendikbudristek for funding this study under contract number 150/UN29.20/PG/2024.

References

[1] H. Sun, P. Saeedi, S. Karuranga, M. Pinkepank, K. Ogurtsova *et al.*, IDF Diabetes Atlas: Global, regional and country-level diabetes prevalence estimates for 2021 and projections for 2045, Diabetes Research and Clinical Practice 183 (2022) 109119.

[2] J. Butayeva, Z. A. Ratan, S. Downie, and H. Hosseinzadeh, The impact of health literacy interventions on glycemic control and self-management outcomes among type 2 diabetes mellitus: A systematic review, Journal of Diabetes 15 (2023) 724-735.

[3] Z. Wang, R. Li, X. Chen, H. Ren, C. Wang *et al.*, Network pharmacology, molecular docking and experimental validation to elucidate the anti-T2DM mechanism of Lanxangia tsaoko, Fitoterapia 178 (2024) 106117.

[4] P. Majety, F. A. Lozada Orquera, D. Edem, and O. Hamdy, Pharmacological approaches to the prevention of type 2 diabetes mellitus, (in English), Front Endocrinol 14 (2023) 1118848.

[5] J. Su, Y. Luo, S. Hu, L. Tang, and S. Ouyang, Advances in Research on Type 2 Diabetes Mellitus Targets and Therapeutic Agents, International Journal of Molecular Sciences 24 (2023) 13381.

[6] X. Meng, X. Liu, J. Tan, Q. Sheng, D. Zhang *et al.*, From Xiaoke to diabetes mellitus: a review of the research progress in traditional Chinese medicine for diabetes mellitus treatment, Chinese Medicine 18 (2023) 75.

[7] A. K. Kandeda, S. Nodeina, and S. T. Mabou, An aqueous extract of Syzygium cumini protects against kainate-induced status epilepticus and amnesia: evidence for antioxidant and anti-inflammatory intervention, Metabolic Brain Disease 37 (2022) 2581-2602.

[8] M. Abdin, Y. S. Hamed, H. M. S. Akhtar, D. Chen, G. Chen *et al.*, Antioxidant and anti-inflammatory activities of target anthocyanins di-glucosides isolated from Syzygium cumini pulp by high speed counter-current chromatography, Journal of Food Biochemistry 44 (2020) e13209.

[9] B. Singh, J. P. Singh, A. Kaur, and N. Singh, Insights into the phenolic compounds present in jambolan (Syzygium cumini) along with their health-promoting effects, International Journal of Food Science & Technology 53 (2018) 2431-2447.

[10] S. Srivastava and D. Chandra, Pharmacological potentials of Syzygium cumini: a review, Journal of the Science of Food and Agriculture 93 (2013) 2084-2093.

[11] S. Li and B. Zhang, Traditional Chinese medicine network pharmacology: theory, methodology and application, Chinese Journal of Natural Medicines 11 (2013) 110-120.

[12] S. R. Morais and A. K, Unlocking the therapeutic potential of nolatrexed in glioblastoma multiforme through quantum mechanics, network pharmacology, molecular docking and ADMET analysis, (in en), Turkish Computational and Theoretical Chemistry 9 96-110.

[13] M. S. Zubair, S. Maulana, A. Widodo, R. Pitopang, M. Arba, and M. Hariono, GC-MS, LC-MS/MS, docking and molecular dynamics approaches to identify potential SARS-CoV-2 3-chymotrypsin-like protease inhibitors from *Zingiber officinale* Roscoe, Molecules 26 (2021) 5230.

[14] A. Daina, O. Michielin, and V. Zoete, SwissADME: a free web tool to evaluate pharmacokinetics, drug-likeness and medicinal chemistry friendliness of small molecules, Scientific Reports 7 (2017) 42717.

[15] A. Daina, O. Michielin, and V. Zoete, SwissTargetPrediction: updated data and new features for efficient prediction of protein targets of small molecules, Nucleic Acids Research 47 (2019) W357-W364.

[16] M. J. Keiser, B. L. Roth, B. N. Armbruster, P. Ernsberger, J. J. Irwin, and B. K. Shoichet, Relating protein pharmacology by ligand chemistry, Nature Biotechnology 25 (2007) 197-206.

[17] M. Rebhan, V. Chalifa-Caspi, J. Prilusky, and D. Lancet, GeneCards: a novel functional genomics compendium with automated data mining and query reformulation support, Bioinformatics 14 (1998) 656-664.

[18] J. S. Amberger, C. A. Bocchini, F. Schiettecatte, A. F. Scott, and A. Hamosh, OMIM.org: Online Mendelian Inheritance in Man (OMIM®), an online catalog of human genes and genetic disorders, Nucleic Acids Research 43 (2015) D789-D798.

[19] J. Piñero, J. Saüch, F. Sanz, and L. I. Furlong, The DisGeNET cytoscape app: Exploring and visualizing disease genomics data, Computational and Structural Biotechnology Journal 19 (2021) 2960-2967.

[20] L.-R. Jiang, Y. Qin, J.-L. Nong, and H. An, Network pharmacology analysis of pharmacological mechanisms underlying the anti-type 2 diabetes mellitus effect of guava leaf, Arabian Journal of Chemistry 14 (2021) 103143.

[21] P. Shannon, A. Markiel, O. Ozier, N. S. Baliga, J. T. Wang *et al.*, Cytoscape: A Software Environment for Integrated Models of Biomolecular Interaction Networks, Genome Research10.1101/gr.1239303 13 (2003) 2498-2504.

[22] M. Kanehisa, M. Furumichi, M. Tanabe, Y. Sato, and K. Morishima, KEGG: new perspectives on genomes, pathways, diseases and drugs, Nucleic Acids Research 45 (2017) D353-D361.

[23] Y. Zhou, B. Zhou, L. Pache, M. Chang, A. H. Khodabakhshi *et al.*, Metascape provides a biologist-oriented resource for the analysis of systems-level datasets, Nature Communications 10 (2019) 1523.

[24] S. X. Ge, D. Jung, and R. Yao, ShinyGO: a graphical gene-set enrichment tool for animals and plants, Bioinformatics 36 (2020) 2628-2629.

[25] G. M. Sastry, M. Adzhigirey, T. Day, R. Annabhimoju, and W. Sherman, Protein and ligand preparation: parameters, protocols, and influence on virtual screening enrichments, Journal of Computer-Aided Molecular Design 27 (2013) 221-34.

[26] M. Arba, S. T. Wahyudi, D. J. Brunt, N. Paradis, and C. Wu, Mechanistic insight on the remdesivir binding to RNA-Dependent RNA polymerase (RdRp) of SARS-cov-2, Computers in Biology and Medicine 129 (2021) 104156.

[27] D. C. Patel, K. R. Hausman, M. Arba, A. Tran, P. M. Lakernick, and C. Wu, Novel inhibitors to ADP ribose phosphatase of SARS-CoV-2 identified by structure-based high throughput virtual screening and molecular dynamics simulations, Computers in Biology and Medicine 140 (2022) 105084.

[28] S. Kumar, S., A. Sajeli Begum, K. Hira, S. Niazi, B. R. Prashantha Kumar *et al.*, Structure-based design and synthesis of new 4-methylcoumarin-based lignans as pro-inflammatory cytokines (TNF-α, IL-6 and

IL-1β) inhibitors, Bioorganic Chemistry 89 (2019) 102991.

[29] Q. Dong, G. Ren, Y. Li, and D. Hao, Network pharmacology analysis and experimental validation to explore the mechanism of kaempferol in the treatment of osteoporosis, Scientific Reports 14 (2024) 7088.

[30] S. W. Vetter, Chapter Five - Glycated Serum Albumin and AGE Receptors, in Advances in Clinical Chemistry, vol. 72, G. S. Makowski, Ed.: Elsevier, 2015, 205-275.

[31] D. Sanajou, A. Ghorbani Haghjo, H. Argani, and S. Aslani, AGE-RAGE axis blockade in diabetic nephropathy: Current status and future directions, European Journal of Pharmacology 833 (2018) 158-164.

[32] X. Wen, C. Lv, R. Zhou, Y. Wang, X. Zhou, and S. Qin, The Molecular Mechanism Underlying the Therapeutic Effect of Dihydromyricetin on Type 2 Diabetes Mellitus Based on Network Pharmacology, Molecular Docking, and Transcriptomics, *Foods* 13 20242. doi: 10.3390/foods13020344

[33] K. Taguchi and K. Fukami, RAGE signaling regulates the progression of diabetic complications, Frontiers in PharmacologyReview 14 (2023).

[34] T. Lanez, A. Yahiaoui, N. Benyza, A. Messai, and L. Elhafnaoui, In silico research on Novel Derivatives of N-(Acetylphenyl)-N-Ferrocenylmethyl-3-nitroaniline as DNA Binding Agents: Using Diverse Computational Methods, including Molecular Docking and ADME/Toxicity Assessment, (in en), Turkish Computational and Theoretical Chemistry 8 (2024) 93-102.

[35] O. Ünsalan, T. Ertan-bolelli, K. Bolelli, C. Altunayar-unsalan, and B. Yılmaz, Effects of flavonoids on SARS–CoV–2 main protease (6W63): A molecular docking study, (in en), Turkish Computational and Theoretical Chemistry 7 (2023) 34-57.

[36] M. Aswad, R. Nugraha, and R. Yulianty, Potency of Bisindoles from Caulerpa racemosa in Handling Diabetes-Related Complications: In silico ADMET Properties and Molecular Docking Simulations, (in en), Turkish Computational and Theoretical Chemistry 8 (2024) 99-107.

[37] E. Edache, A. Uzairu, P. A. Mamza, and G. A. Shallangwa, Investigation of salicylidene acylhydrazides derivatives: Molecular Docking, ADMET, and Molecular Dynamic Simulations were used in conjunction towards the design of new Yersinia pseudotuberculosis inhibitors, (in en), Turkish Computational and Theoretical Chemistry 6 (2022) 9-30.

Supplymantery data

Table S1: Compounds identified from S. cumini extract as revealed by HR-LCMS analysis.

Table S2: The drug-likeness of all compounds

Figure S1: The core targets based on (a) degree, (b) betweeness, (c) closenees.

Figure S2: The top 10 enriched terms for biological process (BP) (a), cellular component (CC) (b), and molecular function (MF) (c) ranked by p-value.

Figure S3: The docked conformations of 3 compounds to IL-6.

Figure S4: The docked conformations of 4 compounds to TNF-α.

Table S1: Compounds identified from *S. cumini* extract as revealed by HR-LCMS analysis. Compounds violated more than one Lipinsky rule of 5 was assigned as red colors.

No	Compound	Molecular Formula	m/z	RT (min)
1	(2S,4R,5S,6S,7R)-5,6,12,14-tetrahydroxy-4-(hydroxymethyl)-13-methoxy-3,8-dioxatricyclo[8.4.0.0²,⁷]tetradeca-1(10),11,13-trien-9-one ATAU bergenin.	$C_{14}H_{16}O_9$	329.08707	5.18
2	(4aS,6aS,6bR,8aR,13aR,13bR,15bS)-N-Benzyl-2,2,6a,6b,9,9,13a-heptamethyl-1,2,3,4,5,6,6a,6b,7,8,8a,9,11,13,13,13b,14,15b-octadecahydro-4aH-chryseno[1,2-f]indazole-4a-carboxamide	$C_{38}H_{53}N_3O$	568.42810	32.49
3	1,2,3,4-Tetrahydroisoquinoline-1-acetic acid	$C_{11}H_{13}NO_2$	224.12837	0.76
4	18-β-Glycyrrhetinic acid	$C_{30}H_{46}O_4$	471.34756	22.56
5	2,5-Bis[(2-acetamidobenzoyl)amino]-1,2,5,6-tetradeoxy-1,6-diphenyl-L-altritol	$C_{36}H_{38}N_4O_6$	623.28674	31.55
6	2-(Cyclopropylmethyl)guanidine	$C_5H_{11}N_3$	114.10272	38.7
7	3,4-MDPA	$C_{13}H_{19}NO_2$	222.14917	0.81
8	3-O-trans-p-Coumaroyltormentic acid	$C_{39}H_{54}O_7$	635.39484	21.95

9	4-(4-methylpiperidin-1-yl)benzoic acid	$C_{13}H_{17}NO_2$	220.13347	0.76
10	5,6-dimethoxy-2-(2-methoxyphenyl)-4H-chromen-4-one	$C_{18}H_{16}O_5$	313.10736	19.79
11	5-Hydroxy-3,4-dimethyl-5-pentyl-2(5H)-furanone	$C_{11}H_{18}O_3$	181.12238	11.19
12	5K8ξ641G3	$C_6H_{10}N_2$	111.09181	38.11
13	6-[(8Z)-8-Octadecen-1-yl]-4-(2-oxo-2-phenylethyl)-2-phenyl-6,7-dihydro-4H-pyrazolo[1,5-a]pyrrolo[3,4-d]pyrimidine-5,8-dione	$C_{40}H_{50}N_4O_3$	635.39514	21.88
14	Amidinomycin	$C_9H_{18}N_4O$	199.15550	13.37
15	Bis(methylbenzylidene)sorbitol	$C_{22}H_{26}O_6$	387.18060	16.89
16	Butyl-(4,5-dihydro-thiazol-2-yl)-amine	$C_7H_{14}N_2S$	159.09518	0.15
17	Chromic acid	H_2CrO_4	118.94273	1.08
18	Cyprodenate	$C_{13}H_{25}NO_2$	228.19601	30.31
19	Dichloroacetic acid	$C_2H_2Cl_2O_2$	128.95094	1.03
20	Dihydroethoxyquin	$C_{14}H_{21}NO$	220.16988	0.84
21	Eglumetad	$C_8H_{11}NO_4$	186.07623	0.76
22	FF-MAS	$C_{29}H_{46}O$	411.36258	27.83
23	N,N,N′,N′-Tetramethylpiperazine-1,4-dicarboxamide	$C_{10}H_{20}N_4O_2$	229.16623	1.07
24	N,N-Diethyloctadecanamide	$C_{22}H_{45}N$	340.35803	36.07
25	N-[(1R)-1-{5-[(1S)-1-Formamido-2-(1H-indol-3-yl)ethyl]-4-(4-methoxybenzyl)-4H-1,2,4-triazol-3-yl}-2-(1H-indol-3-yl)ethyl]-2-pyridinecarboxamide	$C_{37}H_{34}N_8O_3$	639.28217	31.33
26	N-[1-(3-Fluoro-4-methoxyphenyl)butyl]-2-{[(2S)-1-hydroxy-2-propanyl]amino}-5,8-dihydropyrido[3,4-d]pyrimidine-7(6H)-carboxamide	$C_{22}H_{30}FN_5O_3$	432.23843	16.9
27	N-Formylalanine	$C_4H_7NO_3$	118.05000	0.75
28	N-Tridecylglycyl-N-(4-aminobutyl)glycyl-N_2-(tetrahydro-2-furanylmethyl)glycinamide	$C_{28}H_{55}N_5O_4$	526.43231	26.91
29	N-{(1S,2S,4R)-1-[(2,3-Dihydro-1′H-spiro[indene-1,4′-piperidin]-1′-ylsulfonyl)methyl]-7,7-dimethylbicyclo[2.2.1]hept-2-yl}-Nα,Nα-dimethyl-D-histidinamide (Comp29)	$C_{31}H_{45}N_5O_3S$	568.33435	32.45
30	NP-012381	$C_{24}H_{26}O_{10}$	475.16052	14.29
31	NP-017152	$C_{13}H_{23}NO_2$	226.18045	29.91

32	NP-021050	$C_{30}H_{48}O_4$	473.36316	22.97
33	N_1-(Dispiro[cyclohexane-1,3′-[1,2,4,5]tetroxane-6′,2″-tricyclo[3.3.1.1^{3,7}]decan]-4-ylmethyl)-N_4-(6-methoxy-5-phenyl-8-quinolinyl)-1,4-pentanediamine	$C_{38}H_{49}N_3O_5$	628.37549	34.64
34	Tetrahydrofurfuryl methacrylate	$C_9H_{14}O_3$	171.10185	21.68
35	Triazabicyclodecene	$C_7H_{13}N_3$	140.11839	38.11
36	Ursolic acid	$C_{30}H_{48}O_3$	439.35742	27.82
37	N-Ethyl-N-methylcathinone	$C_{12}H_{17}NO$		38.11
38	N-cyclooctylurea	$C_9H_{18}N_2O$		0.43
39	1-tetradecylamine	$C_{14}H_{31}N$		15.92
40	1-[3-(4-Benzyl-1-piperidinyl)propyl]-3(12-oxo-6,7,8,9,10,12 hexahydroazepino[2,1-b]quinazolin-2-yl)thiourea	$C_{29}H_{37}N_5OS$		33.46
41	1,3-Dicyclohexylurea	$C_{13}H_{24}N_2O$		0.17
42	1-(3-Hexyl-4-oxo-2-oxetanyl)-2-tridecanyl N-{[(2-methyl-2-propanyl)oxy]carbonyl}leucinate	$C_{33}H_{61}NO_6$		32.54

Table S2: The drug-likeness properties of all compounds. Compounds violated more than one Lipinsky rule of 5 was assigned as red colors.

No	Compound	Molecular Formula	Lipinski Rule of 5	MW (g/mol)	MlogP	Hbond Aceptor	Hbond Donor
1	(2S,4R,5S,6S,7R)-5,6,12,14-tetrahydroxy-4-(hydroxymethyl)-13-methoxy-3,8-dioxatricyclo[8.4.0.0^{2,7}]tetradeca-1(10),11,13-trien-9-one ATAU bergenin.	$C_{14}H_{16}O_9$	0 Violation	328.27 g/mol	-1.67	9	5
2	(4aS,6aS,6bR,8aR,13aR,13bR,15bS)-N-Benzyl-2,2,6a,6b,9,9,13a-heptamethyl-1,2,3,4,5,6,6a,6b,7,8,8a,9,11,13,13a,13b,14,15b-octadecahydro-4aH-chryseno[1,2-f]indazole-4a-carboxamide	$C_{38}H_{53}N_3O$	2 Violation	567.85 g/mol	6.36	2	2
3	1,2,3,4-Tetrahydroisoquinoline-1-acetic acid	$C_{11}H_{13}NO_2$	0 Violation	191.23 g/mol	1.30	3	2

4	18-β-Glycyrrhetinic acid	$C_{30}H_{46}O_4$	1 Violation	470.68 g/mol	4.87	4	2
5	2,5-Bis[(2-acetamidobenzoyl)amino]-1,2,5,6-tetradeoxy-1,6-diphenyl-L-altritol	$C_{36}H_{38}N_4O_6$	2 Violation	622.71 g/mol	2.50	6	6
6	2-(Cyclopropylmethyl)guanidine	$C_5H_{11}N_3$	0 Violation	113.16 g/mol	0.03	1	2
7	3,4-MDPA	$C_{13}H_{19}NO_2$	0 Violation	221.30 g/mol	2.08	3	1
8	3-O-trans-p-Coumaroyltormentic acid	$C_{39}H_{54}O_7$	2 Violation	634.84 g/mol	4.81	7	4
9	4-(4-methylpiperidin-1-yl)benzoic acid (Comp9)	$C_{13}H_{17}NO_2$	0 Violation	219.28 g/mol	2.39	2	1
10	5,6-dimethoxy-2-(2-methoxyphenyl)-4H-chromen-4-one	$C_{18}H_{16}O_5$	0 Violation	312.32 g/mol	1.25	5	0
11	5-Hydroxy-3,4-dimethyl-5-pentyl-2(5H)-furanone	$C_{11}H_{18}O_3$	0 Violation	198.26 g/mol	1.90	3	1
12	5K8ξ641G3	$C_6H_{10}N_2$	0 Violation	110.16 g/mol	0.32	1	1
13	6-[(8Z)-8-Octadecen-1-yl]-4-(2-oxo-2-phenylethyl)-2-phenyl-6,7-dihydro-4H-pyrazolo[1,5-a]pyrrolo[3,4-d]pyrimidine-5,8-dione	$C_{40}H_{50}N_4O_3$	2 Violation	634.85 g/mol	5.75	4	0
14	Amidinomycin	$C_9H_{18}N_4O$	0 Violation	198.27 g/mol	-0.38	3	4
15	Bis(methylbenzylidene)sorbitol	$C_{22}H_{26}O_6$	0 Violation	386.44 g/mol	-0.38	6	6
16	Butyl-(4,5-dihydro-thiazol-2-yl)-amine	$C_7H_{14}N_2S$	0 Violation	158.26 g/mo	1.23	1	1
17	Chromic acid	H_2CrO_4	0 Violation	118.01 g/mol	1.23	1	1
18	Cyprodenate	$C_{13}H_{25}NO_2$	0 Violation	227.34 g/mol	2.15	3	0
19	Dichloroacetic acid	$C_2H_2Cl_2O_2$	0 Violation	128.94 g/mol	0.49	2	1
20	Dihydroethoxyquin	$C_{14}H_{21}NO$	0 Violation	219.32 g/mol	2.82	1	1
21	Eglumetad	$C_8H_{11}NO_4$	0 Violation	185.18 g/mol	-2.50	5	3
22	FF-MAS	$C_{29}H_{46}O$	1 Violation	410.67 g/mol	6.53	1	1

23	N,N,N′,N′-Tetramethylpiperazine-1,4-dicarboxamide	$C_{10}H_{20}N_4O_2$	0 Violation	228.29 g/mol	0.33	2	0
24	N,N-Diethyloctadecanamide	$C_{22}H_{45}N$	1 Violation	339.60 g/mol	5.17	1	0
25	N-[(1R)-1-{5-[(1S)-1-Formamido-2-(1H-indol-3-yl)ethyl]-4-(4-methoxybenzyl)-4H-1,2,4-triazol-3-yl}-2-(1H-indol-3-yl)ethyl]-2-pyridinecarboxamide	$C_{37}H_{34}N_8O_3$	2 Violation	638.72 g/mol	2.04	6	4
26	N-[1-(3-Fluoro-4-methoxyphenyl)butyl]-2-{[(2S)-1-hydroxy-2-propanyl]amino}-5,8-dihydropyrido[3,4-d]pyrimidine-7(6H)-carboxamide	$C_{22}H_{30}FN_5O_3$	0 Violation	431.50 g/mol	1.81	6	3
27	N-Formylalanine	$C_4H_7NO_3$	0 Violation	117.10 g/mol	-0.54	3	2
28	N-Tridecylglycyl-N-(4-aminobutyl)glycyl-N_2-(tetrahydro-2-furanylmethyl)glycinamide	$C_{28}H_{55}N_5O_4$	1 Violation	525.77 g/mol	0.88	6	3
29	N-{(1S,2S,4R)-1-[(2,3-Dihydro-1′H-spiro[indene-1,4′-piperidin]-1′-ylsulfonyl)methyl]-7,7-dimethylbicyclo[2.2.1]hept-2-yl}-Nα,Nα-dimethyl-D-histidinamide	$C_{31}H_{45}N_5O_3S$	1 Violation	567.79 g/mo	2.19	6	2
30	NP-012381	$C_{24}H_{26}O_{10}$	0 Violation	474.46 g/mol	-0.31	10	5
31	NP-017152	$C_{13}H_{23}NO_2$	0 Violation	225.33 g/mol	1.93	2	2
32	NP-021050	$C_{30}H_{48}O_4$	1 Violation	472.70 g/mo	4.97	4	3
33	N_1-(Dispiro[cyclohexane-1,3′-[1,2,4,5]tetroxane-6′,2″-tricyclo[3.3.1.1^{3,7}]decan]-4-ylmethyl)-N_4-(6-methoxy-5-phenyl-8-	$C_{38}H_{49}N_3O_5$	2 Violation	627.81 g/mol	5.08	7	2

	quinolinyl)-1,4-pentanediamine						
34	Tetrahydrofurfuryl methacrylate	$C_9H_{14}O_3$	0 Violation	170.21 g/mol	0.90	3	0
35	Triazabicyclodecene	$C_7H_{13}N_3$	0 Violation	139.20 g/mol	0.76	1	1
36	Ursolic acid	$C_{30}H_{48}O_3$	1 Violation	456.70 g/mol	5.82	3	2
37	N-Ethyl-N-methylcathinone	$C_{12}H_{17}NO$	0 Violation	191.27 g/mol	2.05	2	0
38	N-cyclooctylurea	$C_9H_{18}N_2O$	0 Violation	170.25 g/mol	1.41	1	2
39	1-tetradecylamine	$C_{14}H_{31}N$	0 Violation	213.40 g/mol	3.95	1	1
40	1-[3-(4-Benzyl-1-piperidinyl)propyl]-3(12-oxo-6,7,8,9,10,12 hexahydroazepino[2,1-b]quinazolin-2-yl)thiourea	$C_{29}H_{37}N_5OS$	1 Violation	503.70 g/mol	4.05	3	2
41	1,3-Dicyclohexylurea	$C_{13}H_{24}N_2O$	0 Violation	224.34 g/mol	2.56	1	2
42	1-(3-Hexyl-4-oxo-2-oxetanyl)-2-tridecanyl N-{[(2-methyl-2-propanyl)oxy]carbonyl}leucinate	$C_{33}H_{61}NO_6$	2 Violation	567.84 g/mol	5.03	6	1

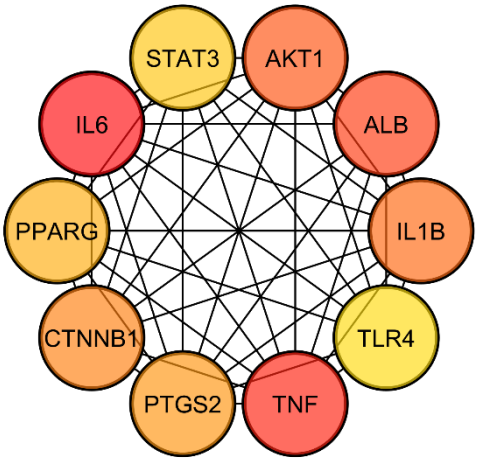

(a)

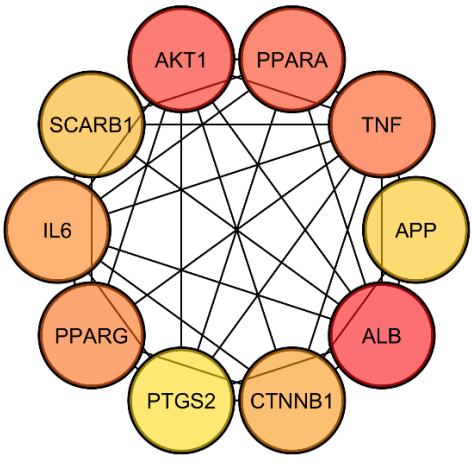

(b)

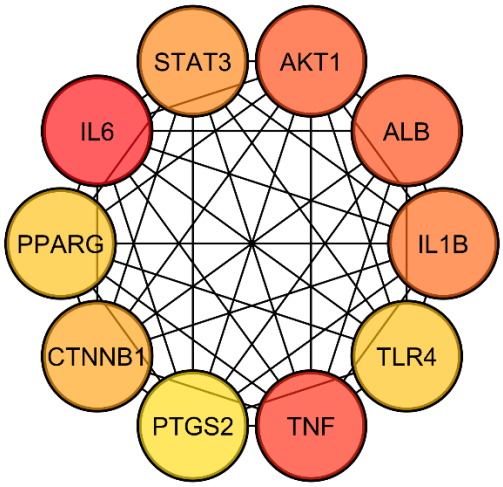

(c)

Figure S1: The core targets based on (a) closenees, (b) betweeness, (c) degree.

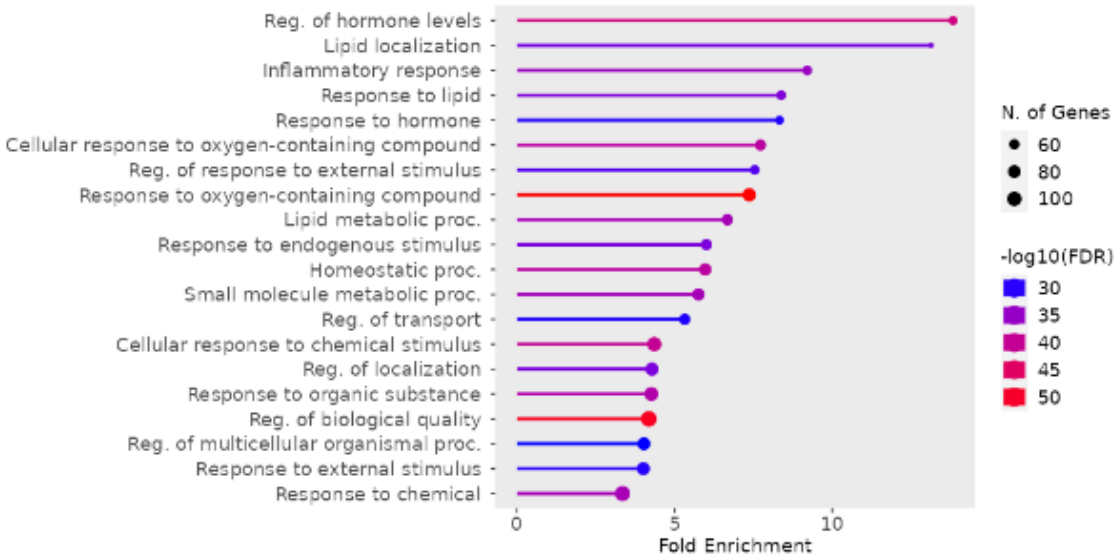

(a)

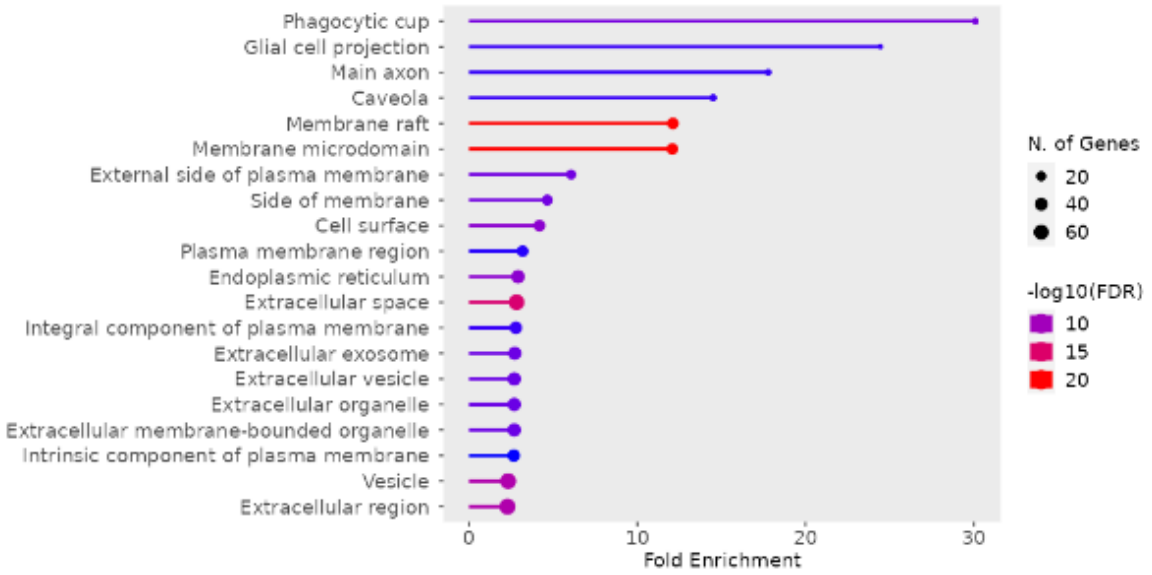

(b)

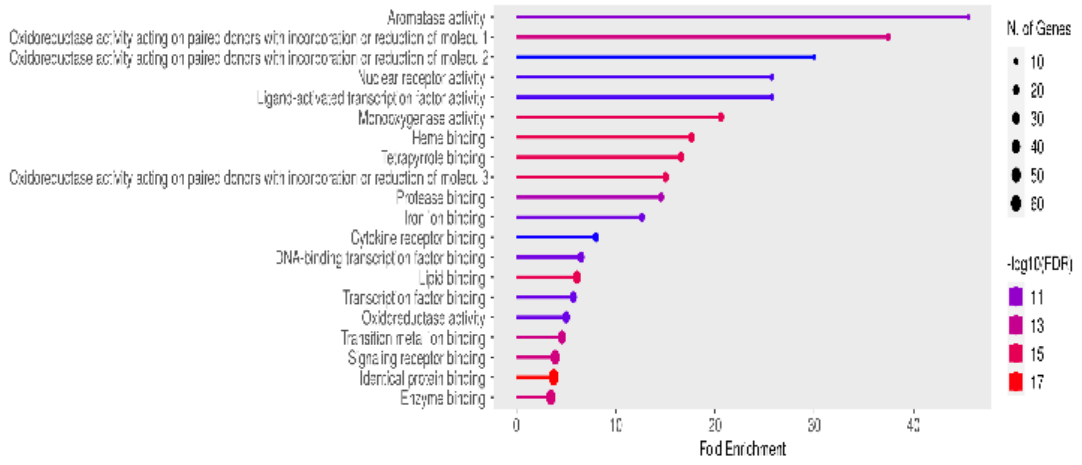

(c)

Figure S2: The top 10 enriched terms for biological process (BP) (a), cellular component (CC) (b), and molecular function (MF) (c) ranked by p-value

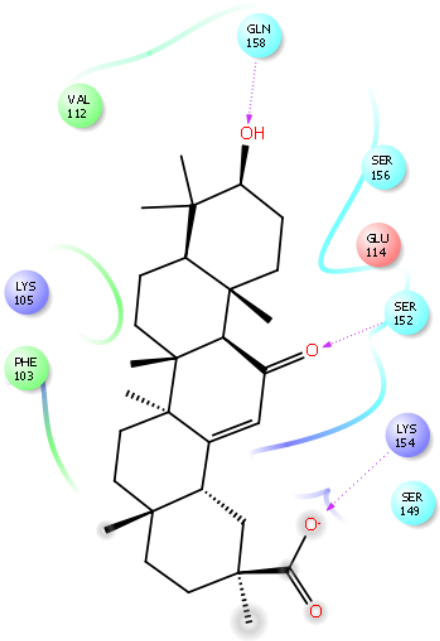

18-β-Glycyrrhetinic acid

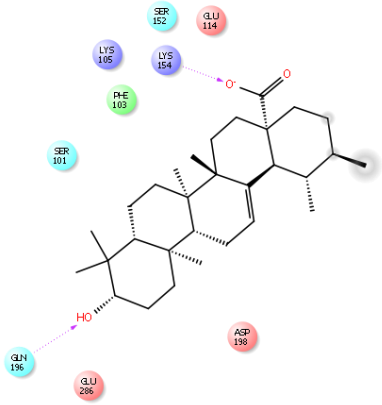

Ursolic acid

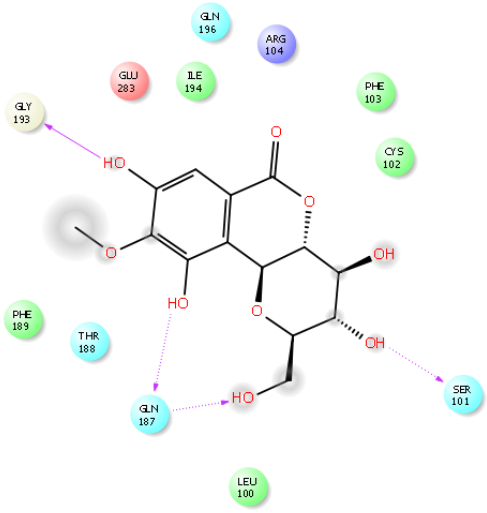

Bergenin

Figure S3: The docked conformations of 3 compounds to IL-6.

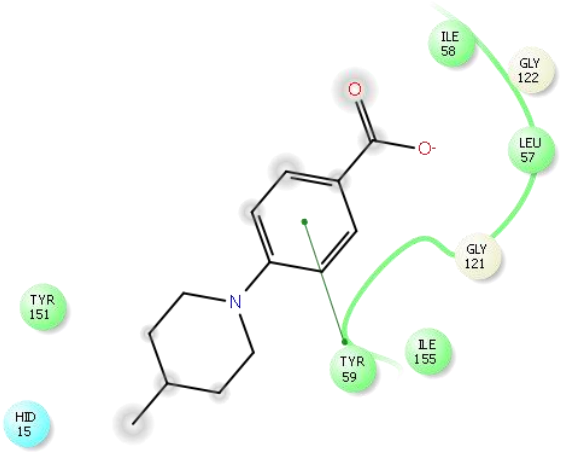

4-(4-methylpiperidin-1-yl)benzoic acid

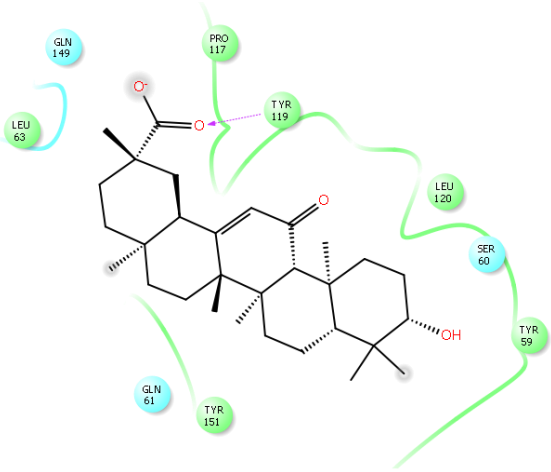

18-β-Glycyrrhetinic acid

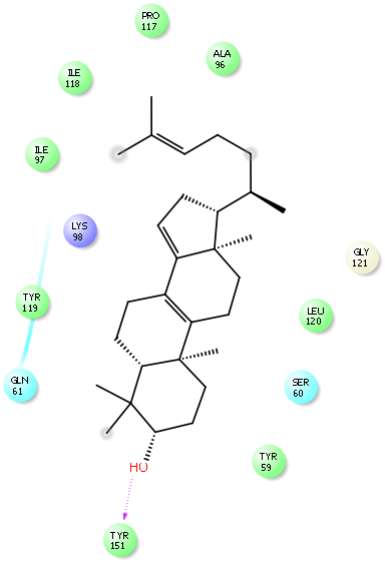

FF-MAS

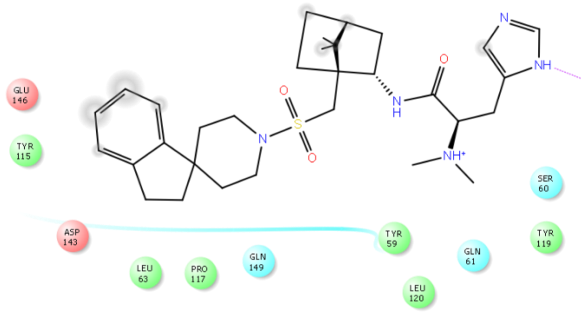

N-{(1S,2S,4R)-1-[(2,3-Dihydro-1′H-spiro[indene-1,4′- piperidin]-1′-ylsulfonyl)methyl]- 7,7-dimethylbicyclo[2.2.1]hept-2-yl}- Nα,Nα-dimethyl-D- histidinamide (Comp29)

Figure S4: The docked conformations of 4 compounds to TNF-α.